Transport properties of a thin GaN channel formed in an Al0.9Ga0.1N/GaN heterostructure grown on AlN/sapphire template

Julien Bassaler, Rémi Comyn, Catherine Bougerol, Yvon Cordier, F Medjdoub, Philippe Ferrandis

Journal of Applied Physics

Transport properties of a thin GaN channel formed in an $Al_{0.9}Ga_{0.1}N$/GaN heterostructure grown on AlN/sapphire template

Cite as: J. Appl. Phys. **131**, 124501 (2022); https://doi.org/10.1063/5.0077107
Submitted: 30 October 2021 • Accepted: 07 March 2022 • Published Online: 24 March 2022

Julien Bassaler, Rémi Comyn, Catherine Bougerol, et al.

Journal of Applied Physics ARTICLE scitation.org/journal/jap

Transport properties of a thin GaN channel formed in an $Al_{0.9}Ga_{0.1}N$/GaN heterostructure grown on AlN/sapphire template

Cite as: J. Appl. Phys. **131**, 124501 (2022); doi: 10.1063/5.0077107
Submitted: 30 October 2021 · Accepted: 7 March 2022 ·
Published Online: 24 March 2022

Julien Bassaler,[1,a)] Rémi Comyn,[2] Catherine Bougerol,[1] Yvon Cordier,[2] Farid Medjdoub,[3] and Philippe Ferrandis[4]

AFFILIATIONS

[1]Univ. Grenoble Alpes, CNRS, Grenoble INP, Institut Néel, 38000 Grenoble, France
[2]Université Côte d'Azur, CNRS, CRHEA, rue Bernard Grégory, 06560 Valbonne, France
[3]CNRS-IEMN, Institute of Electronics, Microelectronics and Nanotechnology, Avenue Poincaré, 59650 Villeneuve d'Ascq, France
[4]Université de Toulon, Univ. Grenoble Alpes, CNRS, Institut Néel, 38000 Grenoble, France

Note: This paper is part of the Special Topic on Defects in Semiconductors.
[a)]**Author to whom correspondence should be addressed:** julien.bassaler@neel.cnrs.fr

ABSTRACT

Despite a high lateral breakdown voltage above 10 kV for large contact distances and a breakdown field of 5 MV cm^{-1} for short contact distances, an $Al_{0.9}Ga_{0.1}N$/GaN heterostructure with an 8 nm strained GaN channel grown on an AlN/sapphire template suffers from a low and anisotropic mobility. This work deals with a material study to elucidate this issue. Threading dislocations were observed along the growth direction in transmission electron microscopy pictures and are more in number in the (11−20) plane. Steps were also detected in this plane at the GaN channel interfaces. With the help of device simulations and static characterizations, the deep level transient spectroscopy technique allowed five traps located in the GaN channel to be identified. Most of them are associated with nitrogen- or gallium-vacancy-related defects and are expected to be localized at the interfaces of GaN with the buffer and the barrier. It is likely that these electrically active defects contribute to reduce the mobility in the two-dimensional electron gas. In addition, a link was established between the mobility and the dependence of the quality of the channel interfaces on the crystallographic orientation.

I. INTRODUCTION

AlGaN/GaN high electron mobility transistors (HEMTs) are promising devices for high voltage applications. Actually, GaN-based HEMTs[1] take advantage of an electron saturation velocity of 2.5×10^7 cm s^{-1}, a breakdown electric field of 3 MV cm^{-1}, and a thermal conductivity of 2.1 W cm^{-1} K^{-1}. A two-dimensional electron gas (2DEG) density around 10^{13} cm^{-2} combined with an electron mobility that can reach 2000 cm^2 V^{-1} s^{-1} also give a major advantage to GaN-based HEMTs.[2]

Despite these interesting properties, the highest withstand voltage of commercially available devices does not exceed 650 V. Many problems limit the device performance in operations like traps and leakage conduction. To address these issues and to achieve operating voltages above kV, several solutions have been explored. The surface passivation was used to reduce surface traps on top of the AlGaN layer, resulting in an increase in the withstand voltage.[3] Field plate engineering was considered to reduce the electric field peaks and avoid the degradation of the device layers.[4] A blocking back barrier allowed a better 2DEG confinement and a reduction of the leakage current toward the substrate.[5] The removal of the substrate was employed to avoid limitations resulting from the substrate material properties.[6]

Another approach is to use a thinner GaN channel sandwiched between ultra-wide bandgap materials. The impact of the substrate and the barrier on the overall breakdown voltage is then reduced.[7] Such a structure has been grown on an AlN/sapphire template, with a strained 8 nm GaN channel and an Al-rich AlGaN barrier. The AlN material with an ultra-wide bandgap of 6.2 eV, a

breakdown electric field[8] of 8.4 MV cm^{-1}, and a thermal conductivity[9] of 2.9 W cm^{-1} K^{-1} is suitable for withstanding high voltages. The performed, i.e. realized AlGaN/GaN heterostructure exhibits a high lateral breakdown voltage above 10 kV for large contact distances and a remarkable breakdown field of 5 MV cm^{-1} for short contact distances.[7] However, the mobility in the 2DEG does not exceed 340 cm^2 V^{-1} s^{-1}. This work aims to find the origin of this low mobility of electrons in the channel.

II. DEVICES FABRICATION

The substrate has an AlN-based structure grown by molecular beam epitaxy (MBE) on sapphire.[7] It is composed of a 6 μm thick commercial AlN-on-sapphire template, a 190 nm AlN buffer, a 8 nm thin GaN channel, a 10 nm AlGaN barrier layer with 90% of the aluminum molar fraction to ensure a high sheet carrier density, and a 5 nm *in situ* grown SiN cap layer. A Transmission Electron Microscopy (TEM) image of the stacking layers is presented in Fig. 1(a). The Ohmic contact was formed with a Ti/Al/Ni/Au metal stack on the top of the barrier layer by etching the SiN cap layer with a fluorine-based plasma. Thermal annealing at 875 °C was then applied to achieve a contact resistance of 0.6 Ω mm. The gate was formed by a Ni/Au metal stack and was deposited on the top of the cap layer.

I–V, C–V, and DLTS measurements were performed on a circular device [Fig. 1(b)] with a gate diameter of 100 μm, an Ohmic ring with a width of 100 μm, and a distance between the gate and Ohmic contacts of 4 μm. Resistivity measurements were realized on the Hall bars [Fig. 1(c)]. The device is 700 μm long and 68 μm wide (W). The distance between contacts 1 and 4 or 2 and 3 is 290 μm (D).

III. EXPERIMENTAL METHOD

The microstructure of the samples was investigated by electron microscopy using a ThermoFischer Tecnai microscope operated at 200 kV. The analyses were performed either in the scanning transmission mode using a high angle annular dark field detector (HAADF-STEM) to emphasize the chemical contrast or using high resolution transmission mode (HR-TEM). The samples were prepared for cross section observations by mechanical polishing followed by ion milling using the Gatan PIPS equipment.

Current–voltage (I–V) and resistivity measurements were performed with a Keithley 2612B source measure unit and capacitance–voltage (C–V) characteristics with an Agilent E4980A precision LCR meter at 1 MHz. The bias was applied between the gate and the Ohmic contact. For the resistivity measurements by four-probe method (4-P), a current from −100 to 100 μA was applied between contacts 5 and 6, and the voltage was measured between contacts 1 and 4 and between contacts 2 and 3. Results come from an average of the measurements of the five Hall bars. All static data were acquired at room temperature in the dark.

From the four-probe measurements, the sheet resistance was determined according to the following equation:

$$R_{sh} = \frac{W}{D} R, \tag{1}$$

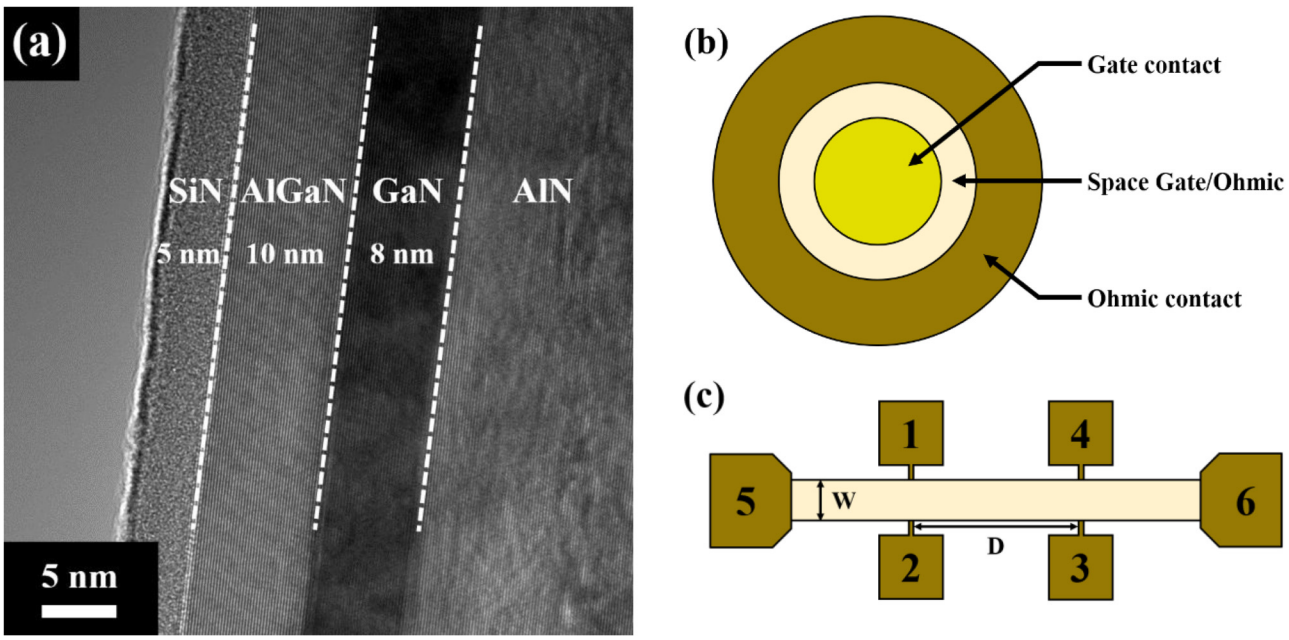

FIG. 1. (a) HR-TEM image of the heterostructure taken at 8° tilt around the [0001] axis from the [10−10] zone axis; (b) schematic top view of the circular device used for I–V, C–V, and DLTS measurements; and (c) schematic top view of the Hall bar with contacts 1–6.

where W and D are the distances defined in Sec. II and R is the resistance determined by the slope of the 4-P characteristic. The electron mobility in the 2DEG μ_n is then determined by

$$\mu_n = \frac{1}{e\, R_{sh}\, n_S}, \tag{2}$$

where e is the electron elementary charge, R_{sh} is the sheet resistance of the 2DEG, and n_S is the 2DEG density.

Simulations of the studied device were made in one and two dimensions with a Schrödinger–Poisson solver, using the Nextnano software. To simplify, only an AlGaN/GaN structure was simulated with a gate metal directly in contact with the barrier layer. A resulting Schottky barrier height of 2 eV for an Al molar fraction of 90% has been calculated from an equation based on the work of Yu *et al.*[11] and used by Ambacher *et al.*[2] This value is consistent with the turn on value of 2 V obtained from I–V measurements (see Sec. IV). The vertical dimensions of the simulated device are similar to the real one (8 nm for the GaN channel and 10 nm for the AlGaN barrier). Due to a calculation deviation for large dimensions, the length of the simulated device was fixed at 60 nm. This does not affect the validity of the simulation since the depletion is mainly vertical and the layer thicknesses are respected. The lateral length of 60 nm is composed of the gate contact with a diameter of 20 nm, two Ohmic contacts of 10 nm length, and the gate-Ohmic distance of 10 nm.

An FT 1030 DLTS system from PhysTech was used to perform DLTS measurements at 1 MHz. The sample was mounted on a thermal stage inside a cryostat. The device was reverse biased with a voltage V_R applied to the gate contact. A pulse voltage V_P was applied to fill the traps during a time t_P. After the end of the pulse voltage, trapped charges are thermally emitted, following the equation

$$e_n = N_C v_{th} \sigma_n \exp\left(\frac{-E_a}{k_B T}\right), \tag{3}$$

where e_n is the thermal emission coefficient of electrons, N_C is the density of states in the conduction band, v_{th} is the thermal electron velocity, σ_n is the apparent electron capture cross section of the trap, E_a is the thermal activation energy of the trap, and k_B is the Boltzmann constant.

Equation (3) can be rewritten as

$$e_n = \gamma_n T^2 \sigma_n \exp\left(\frac{-E_a}{k_B T}\right), \tag{4}$$

where γ_n is given by

$$\gamma_n = \frac{N_C v_{th}}{T^2} = \frac{1}{T^2}\left[2\left(\frac{2\pi m_n^* k_B T}{h^2}\right)^{3/2}\right]\left[\left(\frac{3k_B T}{m_n^*}\right)^{1/2}\right]. \tag{5}$$

Using an electron effective mass in the GaN conduction band of $m_n^* = 0.2\ m_0$,[10] where m_0 is the free electron mass, we calculate $\gamma_n = 6.5 \times 10^{20}\ \mathrm{cm^{-2}\,s^{-1}\,K^{-2}}$. Capacitance transients generated by the thermally emitted charges were recorded from 77 to 500 K between times t_0 and $t_0 + T_W$, where t_0 is the cut-off time and T_W is the period width of the measurement.

IV. STATIC MEASUREMENTS

In Fig. 2(a), we see the capacitance–voltage measurement recorded at 1 MHz. Using the relative permittivities of AlGaN and SiN at $\varepsilon_r(Al_{0.9}Ga_{0.1}N) = 8.6$[12] and $\varepsilon_r(SiN) = 9.4$,[13] respectively, the thickness of the AlGaN/SiN bilayer was calculated at 15.4 nm from the capacitance at 0 V. This value agrees well with the nominal one

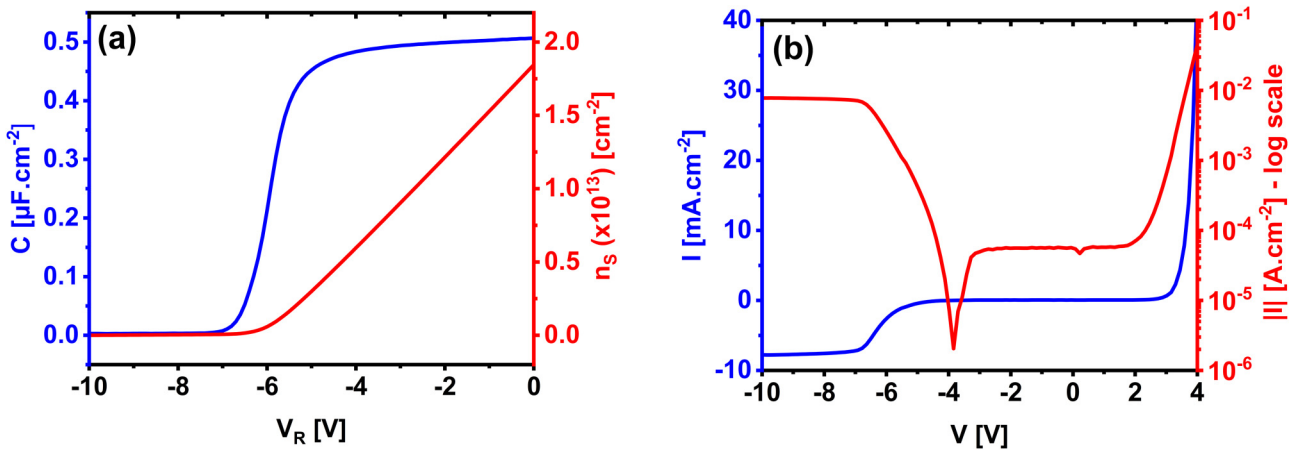

FIG. 2. Static characteristics at room temperature: (a) capacitance–voltage with the corresponding sheet carrier density and (b) current–voltage in linear and logarithmic scales.

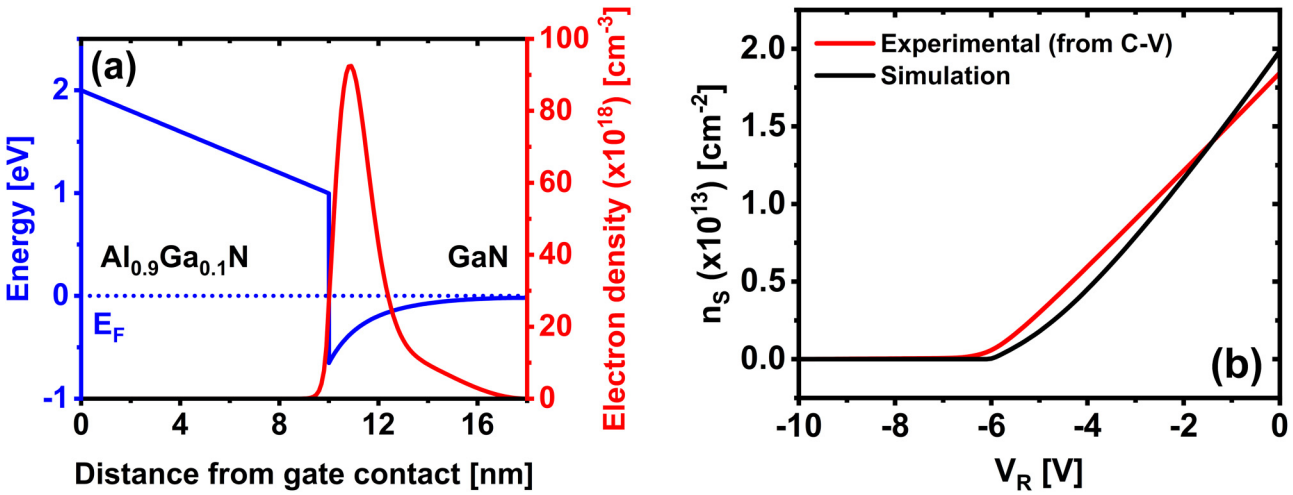

FIG. 3. 1D simulation of (a) the band structure and electron density of the $Al_{0.9}Ga_{0.1}N$/GaN heterostructure and (b) the comparison between the experimental and simulated sheet carrier density evolution as a function of the reverse bias.

of 15 nm. The reduction of the capacitance from 0 to −5.7 V is related to an impoverishment of the 2DEG with an increased drop beyond −4 V. The next regime ($V_R < -5.7$ V) is the depletion where the capacitance reaches almost zero at −7 V, meaning that the 2DEG is fully depleted below the gate contact.

The sheet carrier density of the channel [Fig. 2(a)] was calculated from the C–V measurement by applying the following equation:[14]

$$n_S = \frac{1}{e}\int C.dV, \tag{6}$$

where n_S is the sheet carrier density of the 2DEG, e is the elementary charge, and C is the measured capacitance. A sheet carrier density of 1.8×10^{13} cm^{-2} at 0 V was calculated, agreeing well with the value determined by the Hall effect measurement (1.9×10^{13} cm^{-2}).[7]

The current–voltage characteristic of the device is reported in Fig. 2(b). For a positive voltage, the current seems to follow a diode-like characteristic with a turn on voltage of 2 V. For a reverse bias, the current is first stable at 60 μA/cm^2, then increases from −4 to −7 V, and finally, saturates to 8 mA/cm^2. The more the 2DEG is depleted, the less the current flows through the channel. However, during the same time, a leakage current appears, probably across the SiN passivation.

V. SIMULATIONS

Figure 3(a) reports the 1D simulation of the band structure at the center of the device, below the gate contact. We see from the electron density distribution as a function of the depth that the 2DEG is mainly concentrated in the three-upper nanometer of the GaN layer. In Fig. 3(b), the sheet carrier density n_S obtained from the simulation as a function of the reverse bias is compared to the experimental data. A maximum density of 2.0×10^{13} cm^{-2} at 0 V was determined, agreeing well with the value extracted from the Hall effect and C–V measurements. In addition, the experimental and simulated curves are close to each other for the entire reverse voltage range, which demonstrates the accuracy of the simulation.

The 2D structure was simulated for different gate voltages from 2 to −7 V (Fig. 4). The channel is completely open for 2 V since the Schottky barrier height was fixed to 2 eV. By applying a negative bias on the gate, the channel is progressively impoverished under the gate contact and reaches the depletion regime slightly before −6 V. Beyond this voltage, the channel starts to be laterally depleted toward the gate contact edges. These results are consistent with the static characterizations.

VI. TEM MEASUREMENTS

Transmission electron microscopy (TEM) measurements reported in Fig. 5(a) were acquired along two different planes (11−20) and (10−10). Threading dislocations were identified in the AlN buffer along the growth direction, and we see that they are more in number in the plane (11−20) [Fig. 5(a)].

X-ray diffraction (XRD) using omega scans was previously used to look at the AlN crystal quality.[7] Rocking curve full widths at half maximum (FWHM) around the symmetric AlN (002) reflection and asymmetric AlN (101) reflection peaks were estimated below 350 and 500 arcsec, respectively, indicating a mean threading dislocation density in the range of fewer than 10^8 cm^{-2}. The large lattice mismatch of 13% between AlN and Al_2O_3 is expected to explain the presence of dislocations.[15] Therefore, we cannot exclude the propagation of these dislocations through the GaN channel. In the (11−20) plane, we observe steps, which

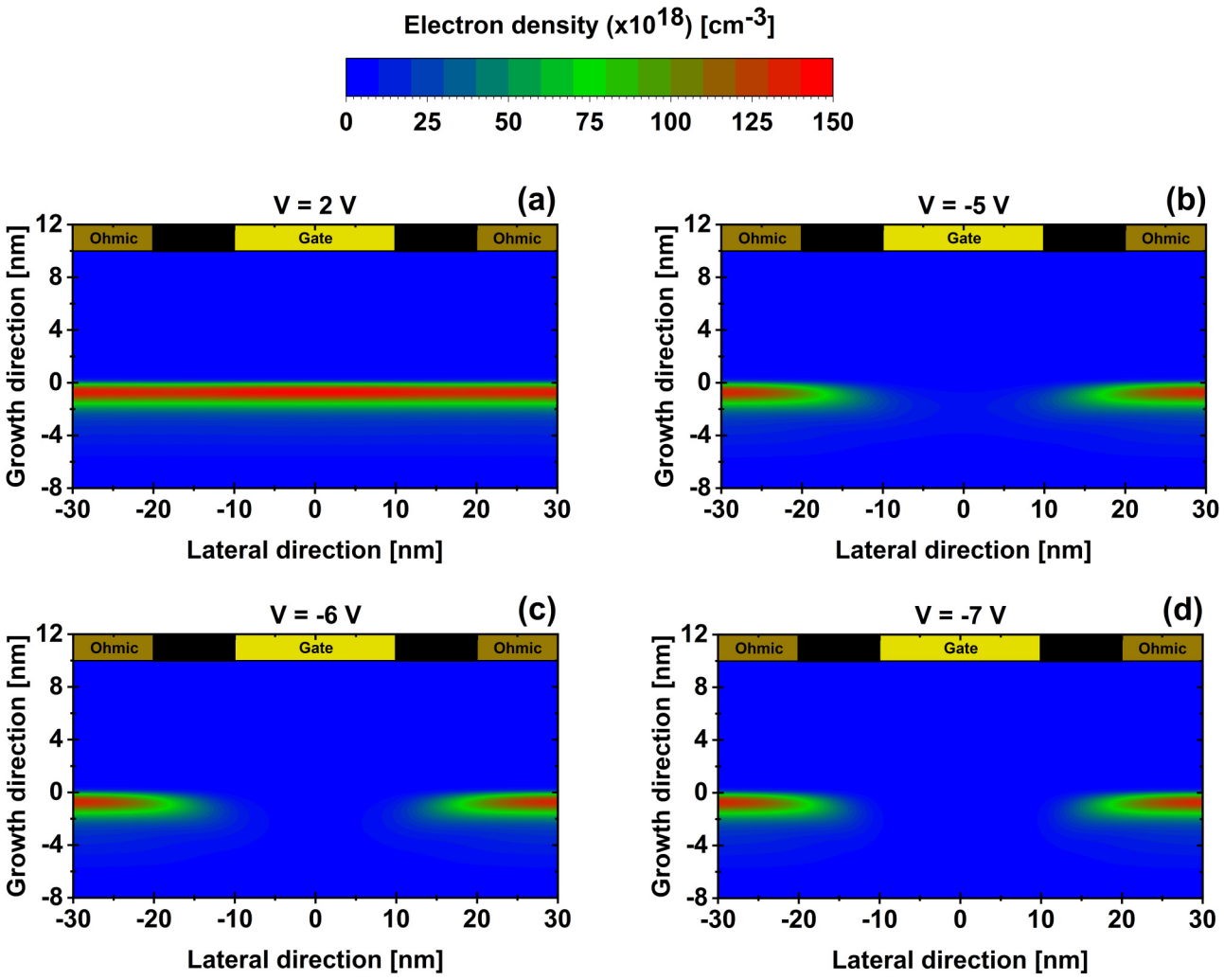

FIG. 4. 2D depletion simulation under the gate contact at different biases of (a) 2, (b) −5, (c) −6, and (d) −7 V.

highlight an interface roughness with the buffer and the barrier [Fig. 5(b)]. Consequently, a link between the roughness of the GaN layer and threading dislocations in the AlN buffer cannot be ruled out. In the (10−10) plane, the shape of the GaN layer seems quite regular and straight but few steps can still be seen on a zoom [the inset of Fig. 5(b)].

VII. DLTS MEASUREMENTS

DLTS measurements were performed by changing the reverse voltage V_R from −1 to −10 V. The pulse voltage V_P was fixed to −0.5 V with a pulse time t_P of 10 ms and a period width T_W of 10 ms. Figure 6(a) reports the DLTS spectra for three different reverse biases at $V_R = -5.4$ V (impoverishment regime), $V_R = -6.0$ V (beginning of the depletion regime), and $V_R = -6.6$ V (near a complete depletion regime below the gate). The capacitance rapidly decreases beyond −5.5 V and reaches zero at −7 V [Fig. 2(a)]. Consequently, only noise is measured on DLTS spectra for V_R beyond −7 V.

In the impoverishment regime, electrons are still present in the triangular well formed at the AlGaN/GaN heterojunction. As a result, the Fermi level is slightly below the GaN conduction band only in the region close to the AlN/GaN interface. Therefore, in this regime, the DLTS signal involves exclusively low deep electron traps E1 and E2. In the depletion regime, the Fermi level is below the conduction band for the entire GaN layer and an electron trap detection can occur in the whole channel thickness. In addition, the Fermi level is low enough to allow the detection of deeper traps (E3, E4, and E5). At $V_R = -6.6$ V, the very weak value of the reverse capacitance below 270 K prevents a trap detection by DLTS [Fig. 6(b)]. Therefore, traps E1 and E2 do not appear in the DLTS spectrum of Fig. 6(a).

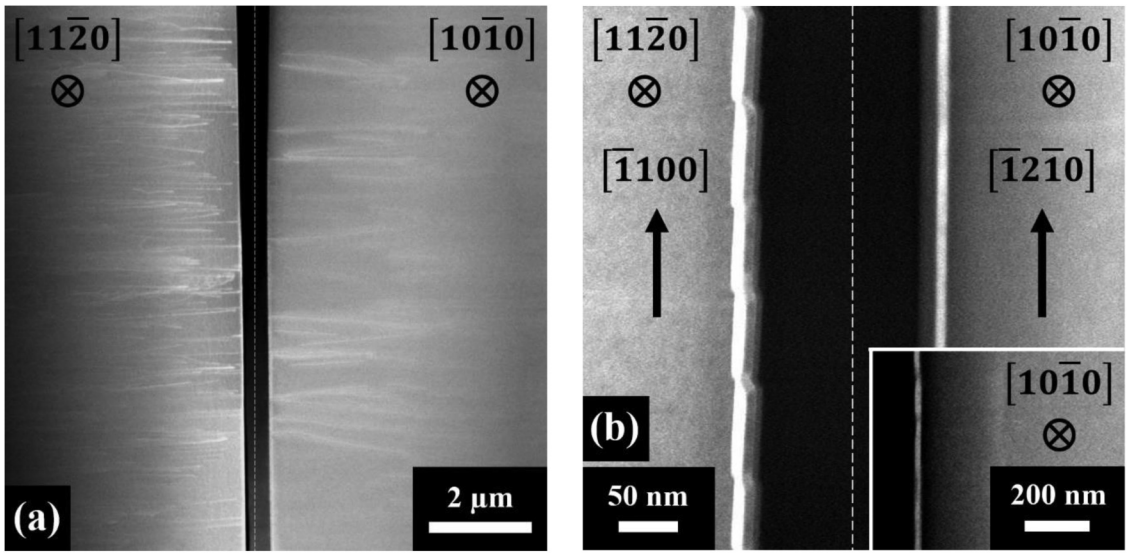

FIG. 5. (a) HAADF-STEM images of a sample cross section, taken in the (11−20) and (10−10) planes, respectively, and (b) zoom of Fig. 5(a) in around the channel region.

Among the five detected traps, we were able to extract the signature of four of them. Trap E3 that appears as a shoulder in the spectrum at $V_R = -5.4$ V does not dominate whatever be the reverse voltage. Therefore, the activation energy and capture cross section of this trap could not be determined. The Arrhenius plots of traps E1, E2, E4, and E5 are reported in Fig. 7, and the extracted values are summarized in Table I.

The activation energies of the traps are in the range 0.14–0.64 eV. Regardless of the voltage applied (V_R or V_P) to the gate, the Fermi level is always away from the conduction band of AlGaN and AlN by more than 1 eV. Hence, the thermal energy even at 500 K remains too weak to allow the detection of traps in the AlGaN barrier and the AlN buffer layer. All deep levels reported in this work are then localized in the GaN channel and have already

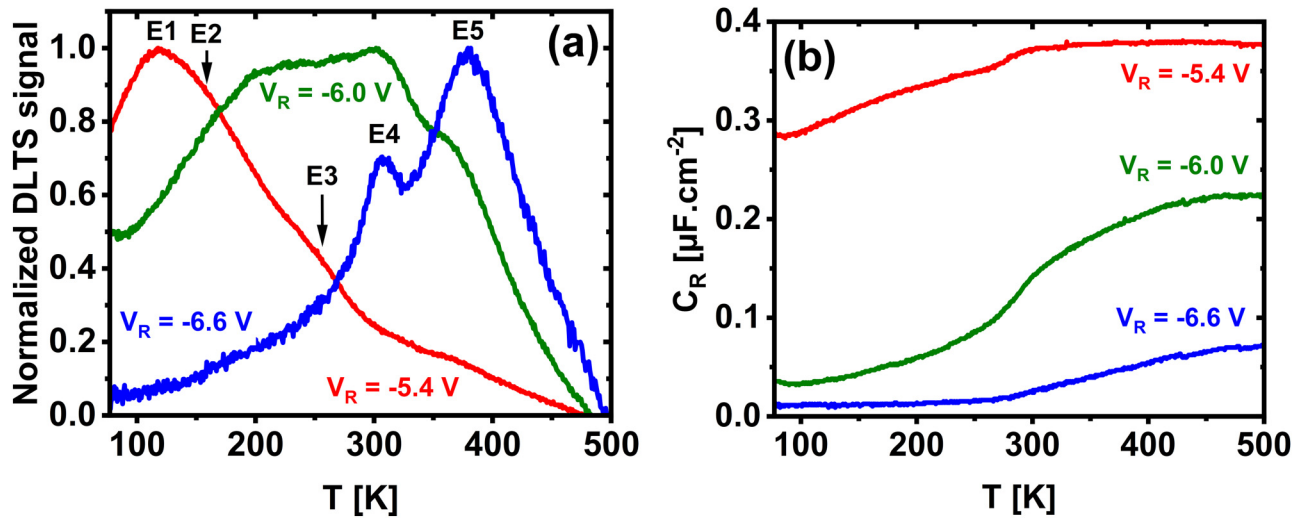

FIG. 6. (a) Normalized DLTS signal at different reverse biases of −5.4, −6.0, and −6.6 V and (b) evolution of the capacitance as a function of temperature for the voltages used for the DLTS measurements.

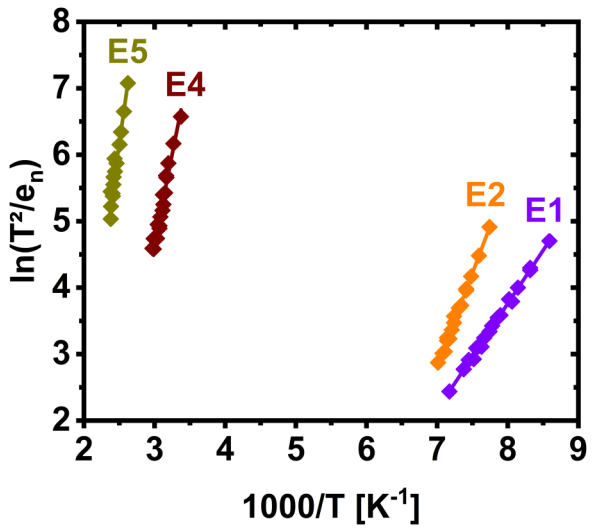

FIG. 7. Arrhenius plots of the detected traps E1, E2, E4, and E5 with a linear fit for each trap.

been detected in GaN-based devices.[14,17,19,20,27–29] They are also commonly observed in GaN grown by MBE.[16,19] Trap E1 is similar to trap E identified by Polenta *et al.*[16] with $E_a = 0.14$ eV and $\sigma_n = 7 \times 10^{-17}$ cm^2. Since irradiation induces this trap, they attributed it to complexes involving a nitrogen-vacancy.[17] E2 is likely related to a complex such as V_N–V_{Ga}.[18] Trap E3, which is between E2 and E4 in DLTS spectra, could correspond to trap C found by Fang *et al.*[19,23,30] and another group[27] with an activation energy of 0.34–0.41 eV and associated with nitrogen-vacancy. E4 could be related to nitrogen-vacancy defects[19,20] or might be associated with dislocations.[17] E5 is associated with gallium-vacancy-related centers.[16,18,19,21–26] Fang *et al.*[29] have shown that most of the traps in thin epitaxial GaN layers with a high dislocation density (10^8–10^9 cm^{-2}) behave as line defects, whereas the same traps in thick GaN layers with lower dislocation density (10^6 cm^{-2}) behave as point defects. However, we conclude that the traps detected in the strained thin GaN layer are similar to traps commonly observed in the relaxed material.

The detection of gallium or nitrogen vacancies related defects could be linked to the roughness of the GaN interfaces observed by TEM analysis. As a break of the lattice periodicity takes place at the heterojunctions, vacancies are likely to occur. In addition, we emphasized that threading dislocations can propagate through the GaN channel, which could possibly explain the detection of trap E4 suspected to be associated with dislocations.

TABLE I. Thermal activation energy; apparent capture cross section; and identification of traps E1, E2, E4, and E5.

Trap	E_a (eV)	σ_n (cm^2)	Identification
E1	0.14 ± 0.01	$(1.28 \pm 0.02) \times 10^{-17}$	V_N related[16,17]
E2	0.24 ± 0.04	$(3.81 \pm 0.08) \times 10^{-14}$	V_N–V_{Ga} complex related[18]
E4	0.46 ± 0.02	$(1.40 \pm 0.10) \times 10^{-16}$	V_N related[19,20] or dislocations[17]
E5	0.64 ± 0.04	$(4.12 \pm 0.37) \times 10^{-16}$	V_{Ga} related[16,18,19,21–26]

TABLE II. Sheet resistance and electron mobility from 4-P measurements on Hall bars along different zone axes.

Crystallographic direction	R_{sh} (Ω)	μ_n (cm^2 V^{-1} s^{-1})
[−12−10]	2419 ± 114	136 ± 14
[01−10]	2280 ± 97	144 ± 14
[11−20]	1795 ± 70	183 ± 17
[10−10]	1683 ± 73	195 ± 19

VIII. MOBILITY DETERMINATION

The sheet resistance and the electron mobility as a function of the orientation of the Hall bars are summarized in Table II. A sheet carrier density value of $n_S = (1.9 \pm 0.1) \times 10^{13}$ cm^{-2} was used to calculate the errors.

In Fig. 8, we can see the axes of the crystal structure used for the TEM images (Fig. 5) and the mobility measurements (Table II). It is worth noting that the mobility is the lowest for directions close to the one where steps were observed by TEM [Fig. 5(b)] and the highest for a perpendicular direction. Therefore, it is absolutely clear that the electron mobility is affected by the roughness of the channel interfaces, and we can assume that the deep electron traps expected to be located at these interfaces play a significant role to break the conduction.

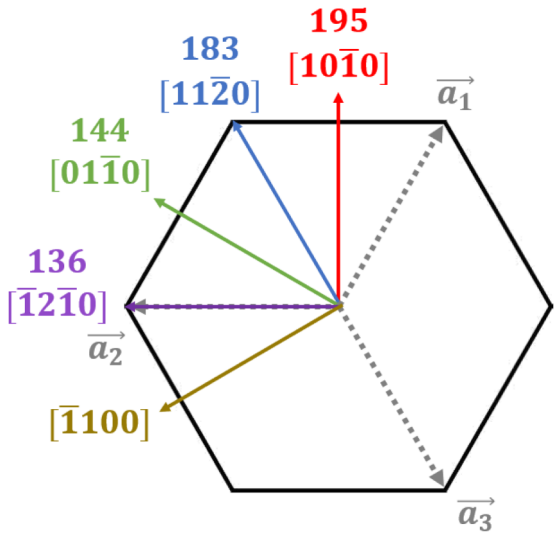

FIG. 8. Crystal structure with different orientations and the corresponding electron mobility in cm^2 V^{-1} s^{-1}.

IX. CONCLUSIONS

An $Al_{0.9}Ga_{0.1}N$/GaN heterostructure with an 8 nm strained GaN channel has been grown on an AlN/sapphire template to address the issue of the withstand voltage for power electronics. A high lateral breakdown voltage up to 10 kV and a breakdown field up to 5 MV cm^{-1} were achieved, but the electron mobility of the device is low and anisotropic. TEM investigations revealed the presence of threading dislocations along the growth axis with a mean density in the AlN buffer estimated below 10^9 cm^{-2} by XRD analysis in the (11−20) plane. A part of them is expected to extend until the thin GaN channel and assumed to be responsible for steps at the interfaces AlN/GaN and $Al_{0.9}Ga_{0.1}N$/GaN. Furthermore, a low and anisotropic mobility between ∼140 and ∼190 $cm^2 V^{-1} s^{-1}$ was determined in the direction or perpendicularly of the steps, respectively. Hence, the interface roughness of the channel leads to reduce the electron mobility by surface scattering. With the help of device simulations and static characterizations, five deep traps with activation energies in the range of 0.14–0.64 eV were detected in the GaN channel by DLTS. Most of them are associated with V_N or V_{Ga} related defects and are expected to be located at the GaN interfaces. The participation of these deep traps in the reduction of the electron mobility in the 2DEG has to be considered. Nevertheless, the $Al_{0.9}Ga_{0.1}N$/GaN heterostructure with the 8 nm thin GaN channel is a promising approach for the next generation of power electronics to address high voltage markets beyond 1200 V. An improvement of the crystal quality of the GaN channel surfaces would allow an increase of the electron mobility to target the high-frequency market as well.

ACKNOWLEDGMENTS

This work was supported by the French National Grant (No. ANR-17-CE05-00131) within the project called BREAKUP and (No. ANR-11-LABX-0014) representing GaNeX: the "Investissements d'Avenir."

AUTHOR DECLARATIONS

Conflict of Interest

The authors have no conflicts to disclose.

Ethics Approval

Ethics approval is not required.

DATA AVAILABILITY

The data that support the findings of this study are available from the corresponding author upon reasonable request.

REFERENCES

[1] *Wide Bandgap Semiconductors: Fundamental Properties and Modern Photonic and Electronic Devices*, edited by K. Takahashi, A. Yoshikawa, and A. Sandhu (Springer-Verlag, Berlin Heidelberg, 2007).
[2] O. Ambacher, J. Smart, J. R. Shealy, N. G. Weimann, K. Chu, M. Murphy, W. J. Schaff, L. F. Eastman, R. Dimitrov, L. Wittmer, M. Stutzmann, W. Rieger, and J. Hilsenbeck, J. Appl. Phys. **85**, 3222 (1999).
[3] B. M. Green, K. K. Chu, E. M. Chumbes, J. A. Smart, J. R. Shealy, and L. F. Eastman, IEEE Electron Device Lett. **21**, 268 (2000).
[4] Y. Ando, Y. Okamoto, H. Miyamoto, T. Nakayama, T. Inoue, and M. Kuzuhara, IEEE Electron Device Lett. **24**, 289 (2003).
[5] H.-C. Lee, S.-Y. Hyun, H.-I. Cho, C. Ostermaier, K.-W. Kim, S.-I. Ahn, K.-I. Na, J.-B. Ha, D.-H. Kwon, C.-K. Hahn, S.-H. Hahm, H.-C. Choi, and J.-H. Lee, Jpn. J. Appl. Phys. **47**, 2824 (2008).
[6] B. Lu and T. Palacios, IEEE Electron Device Lett. **31**, 951 (2010).
[7] I. Abid, R. Kabouche, C. Bougerol, J. Pernot, C. Masante, R. Comyn, Y. Cordier, and F. Medjdoub, Micromachines **10**, 690 (2019).
[8] T. Ruemenapp and D. Peier, in *2000 Eighth International Conference on Dielectric Materials, Measurements and Applications, IEEE Conf.: Publ. No. 473* (IEEE, 2000), pp. 285–290.
[9] G. A. Slack, R. A. Tanzilli, R. O. Pohl, and J. W. Vandersande, J. Phys. Chem. Solids **48**, 641 (1987).
[10] M. E. Levinshtein, S. L. Rumyantsev, and M. S. Shur, *Properties of Advanced Semiconductor Materials: GaN, AIN, InN, BN, SiC, SiGe* (John Wiley & Sons, 2001).
[11] L. S. Yu, D. J. Qiao, Q. J. Xing, S. S. Lau, K. S. Boutros, and J. M. Redwing, Appl. Phys. Lett. **73**, 238 (1998).
[12] R. J. Trew, Proc. IEEE **90**, 1032 (2002).
[13] S. M. Hu, J. Electrochem. Soc. **113**, 693 (1966).
[14] P. Ferrandis, M. Charles, C. Gillot, R. Escoffier, E. Morvan, A. Torres, and G. Reimbold, Microelectron. Eng. **178**, 158 (2017).
[15] J. W. Kim, Y.-H. Hwang, J. H. Cho, and H. K. Kim, Jpn. J. Appl. Phys. **40**, 4677 (2001).
[16] L. Polenta, Z.-Q. Fang, and D. C. Look, Appl. Phys. Lett. **76**, 2086 (2000).
[17] Z.-Q. Fang, L. Polenta, J. W. Hemsky, and D. C. Look, in *2000 International Semiconducting and Insulating Materials Conference, SIMC-XI (Cat. No. 00CH37046)* (IEEE, Canberra, 2000), pp. 35–42.
[18] Z.-Q. Fang, D. C. Look, J. Jasinski, M. Benamara, Z. Liliental-Weber, and R. J. Molnar, Appl. Phys. Lett. **78**, 332 (2001).
[19] Z. Fang, G. Farlow, B. Claflin, and D. Look, in *13th International Conference on Semiconducting and Insulating Materials, 2004, SIMC-XIII-2004* (IEEE, 2004), pp. 29–36.
[20] P. Ferrandis, M. El-Khatib, M.-A. Jaud, E. Morvan, M. Charles, G. Guillot, and G. Bremond, Semicond. Sci. Technol. **34**, 045011 (2019).
[21] P. Hacke, T. Detchprohm, K. Hiramatsu, N. Sawaki, K. Tadatomo, and K. Miyake, J. Appl. Phys. **76**, 304 (1994).
[22] Z.-Q. Fang, D. C. Look, W. Kim, Z. Fan, A. Botchkarev, and H. Morkoç, Appl. Phys. Lett. **72**, 2277 (1998).
[23] Z.-Q. Fang, D. C. Look, P. Visconti, D.-F. Wang, C.-Z. Lu, F. Yun, H. Morkoç, S. S. Park, and K. Y. Lee, Appl. Phys. Lett. **78**, 2178 (2001).
[24] S. Chen, U. Honda, T. Shibata, T. Matsumura, Y. Tokuda, K. Ishikawa, M. Hori, H. Ueda, T. Uesugi, and T. Kachi, J. Appl. Phys. **112**, 053513 (2012).
[25] D. Haase, M. Schmid, W. Kürner, A. Dörnen, V. Härle, F. Scholz, M. Burkard, and H. Schweizer, Appl. Phys. Lett. **69**, 2525 (1996).
[26] C. D. Wang, L. S. Yu, S. S. Lau, E. T. Yu, W. Kim, A. E. Botchkarev, and H. Morkoç, Appl. Phys. Lett. **72**, 1211 (1998).
[27] P. Ferrandis, M. Charles, Y. Baines, J. Buckley, G. Garnier, C. Gillot, and G. Reimbold, Jpn. J. Appl. Phys. **56**, 04CG01 (2017).
[28] P. Ferrandis, M. El-Khatib, M.-A. Jaud, E. Morvan, M. Charles, G. Guillot, and G. Bremond, J. Appl. Phys. **125**, 035702 (2019).
[29] Z.-Q. Fang, D. C. Look, and L. Polenta, J. Phys.: Condens. Matter **14**, 13061 (2002).
[30] Z.-Q. Fang, D. C. Look, X.-L. Wang, J. Han, F. A. Khan, and I. Adesida, Appl. Phys. Lett. **82**, 1562 (2003).